Effect of Stress-dependent Thermal Conductivity on Thermo-mechanical Coupling Behavior in GaN-based Nanofilm under Pulse Heat Source

Qicong Li[1] Xiaoya Tang[1] Linli Zhu [1*] Haihui Ruan[2*]

[1]Department of Engineering Mechanics, and Key Laboratory of Soft Machines and Smart Devices of Zhejiang Province, Zhejiang University, Hangzhou 310027, China

[2]Department of Mechanical Engineering, The Hong Kong Polytechnic University, Hong Kong, China

Abstract

The thermal properties of a nanostructured semiconductor are affected by multi-physical fields, such as stress and electromagnetic fields, causing changes in temperature and strain distributions. In this work, the influence of stress-dependent thermal conductivity on the heat transfer behavior of a GaN-based nanofilm is investigated. The finite element method is adopted to simulate the temperature distribution in a prestressed nanofilm under heat pulses. Numerical results demonstrate the effect of stress field on the thermal conductivity of GaN-based nanofilm, namely, the prestress and the thermal stress lead to a change in the heat transfer behavior in the nanofilm. Under the same heat source, the peak temperature

* Author to whom correspondence should be addressed; electronic mail: llzhu@zju.edu.cn (Linli Zhu) and haihui.ruan@polyu.edu.hk (Haihui Ruan)

of the film with stress-dependent thermal conductivity is significantly lower than that of the film with a constant thermal conductivity, and the maximum temperature difference can reach 8.2 K. These results could be useful for designing GaN-based semiconductor devices with higher reliability under multi-physical fields.

Keywords: Multi-physical effect, Stress-dependent thermal conductivity, Prestress fields, Heat transfer behavior, GaN-based nanofilm, Finite element method

1. Introduction

Semiconductor-based micro/nanoelectronic devices suffer from the multi-physical environment in applications, such as stress, temperature, electromagnetic and radiation fields [1-8]. These physical fields cause changes in the physical properties of nanostructured materials through surface/interface effects and quantum effects [9-16], thus affecting the performance and reliability of micro/nanoelectronic devices. The multi-field coupling leads to temperature and stress/strain distributions in electronic devices [17-24], and the affected material properties cause further changes in the distributions of internal temperature, electric potential, and stress. Such complex thermo-electro-mechanical coupling could cause the failure of semiconductor materials and devices.

Finite element methods have been widely used to analyze the multi-physical coupling behaviors in electronic devices. For example, Calame *et al*. [25] developed a finite element method for thermodynamic simulation to study the microchannel technology for cooling GaN-based high-electron-mobility transistors (HEMTs) and determine the choice of crystalline materials that minimizes temperature and stresses in these devices. Bykhovsk *et al*. [26] conducted finite element simulations and found that the strain-induced electric field changed the voltage threshold of a GaN/AlN/GaN semiconductor-insulator-semiconductor (SIS) structure, leading to an asymmetric charge distribution and asymmetric capacitance-voltage characteristics. Rivera [27] found that the electromechanical performance of a capacitor is affected by the electrostatic force between the electrodes based on thermodynamic calculations. Wang *et al*. [28] studied the transient temperature and thermal stress distributions in copper, polysilicon, and tungsten/polysilicon through-silicon vias (TSV) under pulsed voltage using a modified mixed-time finite element method. Ancona *et al*. [29] established a multi-dimensional continuous coupling model for simulating the thermoelastic behavior of GaN HEMTs based on linear thermo-electro-elastic theory, Fick's law, and the heat-conduction equation. Zhang *et al*. [30] used a well-functioning-hybrid time-domain finite element method to calculate the temperature and thermal stress variations of a multi-gate AlGaN/GaN HEMT device under periodically pulsed power signals. Using the same mixed-time finite element method, Zhang [31] further studied the effect of diamond heat sinks on the static and transient thermal response in AlGaN/GaN HEMTs. It is noted that the effect of stress on thermal conductivity has not been taken into account in existing analyses of the multi-physical coupling behaviors of GaN-based structures, though existing studies have demonstrated that the thermal properties of semiconductor nanostructures are dependent on stress/strain fields [14, 32-37].

In this work, we provide an insight into the temperature response and stress distribution of a stressed-GaN nanofilm under heat pulses. The influence of thermo-mechanical coupling on temperature distribution in GaN-based films is investigated by using the finite element method. Numerical results show that the stress-dependent thermal conductivity causes a change in temperature distribution in the films under a pulsed heat source. The maximum change of temperature could be several degrees. The results obtained in this work would provide theoretical support for designing reliable GaN-based devices under multi-physical fields.

2. Theoretical Description

The effect of a stress field on the phonon and thermal properties of GaN-based nanofilms has been studied comprehensively in our previous work [38-43]. According to these studies, the phonon properties and phonon thermal conductivity under a stress field can be significantly different from those without stress in GaN-based nanostructures, and the effect of stress field on thermal conductivity also depends on temperature [14, 39, 42]**.** Herein, a GaN-based nanofilm with a thickness of 6 nm is taken as an example to reveal the variation in the heat transfer behavior of stressed-nanofilm under a pulsed heat source. Since there is thermal stress in the film under heat pulses, the effects of both mechanical and thermal stresses on thermal conductivity must be considered. The stress-dependent thermal conductivity of GaN-based nanofilm is described in section 2.1. The governing equations for heat transfer and the related weak form are presented in sections 2.2 and 2.3, respectively, which lead to the finite element formulation of determining temperature and stress fields in a stressed nanofilm under heat pulses.

2.1. Stress Coupling Effect on Thermal Conductivity in Semiconductor Nanofilm

The phonon thermal conductivity is one of the most important thermal properties of semiconductor nanomaterials, which can be expressed as:

$$\kappa_{\mathrm{Ph}}=\frac{1}{3}\left(\frac{k_B}{\hbar}\right)k_B T\sum_n\int\frac{x^2\mathrm{e}^x}{\left(\mathrm{e}^x-1\right)^2}f_n\left(x\right)v_n^2\left(x\right)\tau_n\left(x\right)\mathrm{d}x \tag{1}$$

where, $x=\hbar\omega/k_B T$, ω represents a phonon frequency, ħ the Planck constant, k_B the Boltzmann constant, τ_n the phonon relaxation time, T the temperature, and f_n and v_n, respectively, the phonon density of state (DOS) and group velocity for a given number of phonon mode n. The function $f_n(x)$ can be expressed for nanofilm as

$$f_n^{SA,AS,SH}\left(\omega\right)=\frac{1}{H}\left[\frac{1}{2\pi}q_{0n}^{SA,AS,SH}\left(\omega\right)\frac{1}{v_n^{SA,AS,SH}(\omega)}\right] \tag{2}$$

where, SH, SA, and AS denote the shear mode, dilatational mode, and flexural mode for phonons in nanofilm, respectively, H the thickness of the nanofilm, and q_0 the phonon wave vector. The group velocity $v_n(x)$ is expressed as:

$$v_n\left(q_0\right)=\frac{\mathrm{d}\omega_n(q_0)}{\mathrm{d}q_0} \tag{3}$$

Before achieving the phonon group velocity and phonon DOS, the phonon dispersion relation of a nanofilm should be determined. The previous studies have demonstrated that an elastic model can well describe the phonon dispersion relation of nanofilms [44-47]. Based on the elastic model, the eigenvalue equation for phonons is given as [14, 48]

$$\mathbf{D}\hat{u}\left(x_3\right)=-\rho\omega^2\hat{u}\left(x_3\right) \tag{4}$$

where

$$\mathbf{D}=\begin{bmatrix} \bar{C}_{44}\dfrac{\mathrm{d}^2}{\mathrm{d}x_3^2}-C_{11}q_0^2+\dfrac{\mathrm{d}\bar{C}_{44}}{\mathrm{d}x_3}\dfrac{\mathrm{d}}{\mathrm{d}x_3} & 0 & -\mathrm{i}q_0(\bar{C}_{13}+\bar{C}_{44})\dfrac{\mathrm{d}}{\mathrm{d}x_3}-\mathrm{i}q_0\dfrac{\mathrm{d}\bar{C}_{44}}{\mathrm{d}x_3} \\ 0 & \bar{C}_{44}\dfrac{\partial^2}{\partial x_3^2}-\bar{C}_{66}q_0^2+\dfrac{\mathrm{d}\bar{C}_{44}}{\mathrm{d}x_3}\dfrac{\mathrm{d}}{\mathrm{d}x_3} & 0 \\ -\mathrm{i}q_0(\bar{C}_{13}+\bar{C}_{44})\dfrac{\mathrm{d}}{\mathrm{d}x_3}-\mathrm{i}q_0\dfrac{\mathrm{d}\bar{C}_{13}}{\mathrm{d}x_3} & 0 & \bar{C}_{33}\dfrac{\mathrm{d}^2}{\mathrm{d}x_3^2}-\bar{C}_{44}q_0^2+\dfrac{\mathrm{d}\bar{C}_{33}}{\mathrm{d}x_3}\dfrac{\mathrm{d}}{\mathrm{d}x_3} \end{bmatrix} \quad (5)$$

The boundary condition is

$$x_1=\pm\frac{H}{2},\quad \sigma_{13}=\sigma_{23}=\sigma_{33}=0 \quad (6)$$

For the shear (SH) mode, the displacement field is $\hat{u}=(0,u_2,0)$, and the eigenvalue equation of the shear mode can be expressed as

$$\bar{C}_{44}\frac{\mathrm{d}^2\hat{u}_2}{\mathrm{d}x_3^2}+\left[\rho\omega^2-\bar{C}_{66}q_0^2\right]\hat{u}_2=0 \quad (7)$$

For the dilatational (SA) and flexural (AS) modes, $\hat{u}=(u_1,0,u_3)$, the eigenvalue equations are:

$$\begin{cases} \bar{C}_{44}\dfrac{\mathrm{d}^2\hat{u}_1}{\mathrm{d}x_3^2}-\mathrm{i}q_0(\bar{C}_{13}+\bar{C}_{44})\dfrac{\mathrm{d}\hat{u}_3}{\mathrm{d}x_3}+\left[\rho\omega^2-\bar{C}_{11})q_0^2\right]\hat{u}_1=0 \\ \bar{C}_{33}\dfrac{\mathrm{d}^2\hat{u}_3}{\mathrm{d}x_3^2}-\mathrm{i}q_0(\bar{C}_{13}+\bar{C}_{44})\dfrac{\mathrm{d}\hat{u}_1}{\mathrm{d}x_3}+\left[\rho\omega^2-\bar{C}_{44}q_0^2\right]\hat{u}_3=0 \end{cases} \quad (8)$$

Eqs. (7) and (8) can be numerically solved for the phonon dispersion relations of SH, SA, and AS modes.

From the expression for phonon thermal conductivity of a nanofilm, Eq. (1), one can find that the thermal conductivity is related to the phonon group velocity, DOS, and the relaxation time, all of which are the function of phonon frequency. When a prestress field exists, the stress-dependent terms can be involved in the effective elastic modulus in the elastic model given in Eqs. (4)-(8), leading to the stress-dependent phonon frequency. For the GaN-based nanofilms under a prestress field as shown in Fig. 1(a), the calculated phonon thermal conductivities as a function of the applied stress is shown in Fig. 1(b). It is noted that a compressive (tensile) stress increases (decreases) the thermal conductivity. The larger applied stress leads to a more significant change in thermal conductivity. The experimental studies demonstrated that the prestress could be in the order of GPa [49, 50] in nanodevices. These significant prestresses can be induced by the lattice misfit between a nanofilm and a substrate. Therefore, in Fig. 1, the prestress is in the order of GPa, which can cause a significant change in the thermal conductivity.

2.2. Governing Equations of Heat Transfer in a Nanofilm

The temperature distribution in the stressed-nanofilm under a pulsed heat source can be simulated based on the heat transfer equations with prescribed boundary conditions, which is expressed as

$$\nabla \bullet (\kappa_{\mathrm{Ph}} \nabla T) = -(J_e - c\rho \frac{\partial T}{\partial t}) \tag{9}$$

in which κ_{Ph} is the stress-dependent thermal conductivity, J_e an external heat source, c specific heat, and ρ the density of material. Since the thermal conductivity κ_{Ph} is a function of stress, it is no longer a constant before the Laplace operator but needs to be kept in the divergence operator, as shown in Eq. (9). The general boundary conditions of the temperature filed in a nanofilm are summarized as follows. The convective boundary condition is

$$\kappa_{\mathrm{Ph}} \frac{\partial T}{\partial n} |_{M \in S_c} = q_{S_c}(M,t) = -\bar{\beta}(T_{S_c} - T_e) \tag{10}$$

in which $q_{S_c}(M,t)$ is the heat flux from the surrounding medium into the temperature field, $\bar{\beta}$ the convection coefficient, T_{S_c} the temperature of the boundary S_c , and T_e the environment temperature (room temperature unless otherwise specified). M represents a point on the boundaries. The conduction boundary condition is

$$\kappa_{\mathrm{Ph}} \frac{\partial T}{\partial n} |_{M \in S_2} = q_{S_2}(M,t) \tag{11}$$

in which $q_{S_2}(M,t)$ is the heat flux intensity of normal conduction at any point of the conduction boundary S_2 . Here $\partial T / \partial n$ refers to the gradient value of the temperature field along the normal direction of the boundary. The boundary condition with a given temperature is

$$T(M,t)|_{M \in S_1} = \varphi(M,t) \tag{12}$$

Here, φ is the temperature on the boundary S_1. The initial condition can be given as

$$T(x,y)|_{t=0} = T_e \tag{13}$$

i.e., the initial temperature is room temperature.

2.3. Finite Element Formulation of Temperature Field under a Pulsed Heat Source

Based on Eqs. (9)–(13), the finite element formulae of transient temperature distribution can be derived by the variational method. For the region Ω, one can choose a weighted function ψ and apply the Galerkin method to Eq. (9) to obtain

$$\int_{\Omega} \left[\nabla \bullet (\kappa_{\mathrm{Ph}} \nabla T) + J_e - c\rho \frac{\partial T}{\partial t} \right] \delta\psi \mathrm{d}\Omega = 0 \tag{14}$$

Using Gauss theorem and combining with boundary conditions of Eqs. (10 – 12), one can derive

$$\int_{\Gamma_{S_1}} 0\mathrm{d}\Gamma_{S_1} + \int_{\Gamma_{S_2}} q_{S_2}\delta\psi \mathrm{d}\Gamma_{S_2} + \int_{\Gamma_{S_c}} -\bar{\beta}(T_{S_c} - T_e)\delta\psi \mathrm{d}\Gamma_{S_c}$$

$$+\int_{\Omega}[(c\rho\frac{\partial T}{\partial t} - J_e)]\delta\psi \mathrm{d}\Omega + \int_{\Omega}[\kappa_{\mathrm{Ph}}(\frac{\partial T}{\partial x}\frac{\partial\delta\psi}{\partial x} + \frac{\partial T}{\partial y}\frac{\partial\delta\psi}{\partial y})]\mathrm{d}\Omega = 0 \tag{15}$$

Choosing a trial function $\psi = T$ and marking the shape functions of an element as $[N^{et}]_e = [N^{et}(x, y)]_e$, the finite element formula of transient temperature distribution is obtained as:

$$[C^{et}]_e[\frac{\partial T}{\partial t}]_e + [K^{et}]_e[T]_e = [R^{et}]_e \tag{16}$$

in which

$$\begin{cases} [C^{et}]_e = \int_{Se}([N^{et}]_e)^T c\rho[N^{et}]_e H\mathrm{d}S \\ [K^{et}]_e = [K_T^{et}]_e + [K_c^{et}]_e \\ [R^{et}]_e = [R_B^{et}]_e + [R_c^{et}]_e + [R_s^{et}]_e \end{cases} \tag{17}$$

Here, $[K_T^{et}]_e$ and $[K_c^{et}]_e$ are conduction matrix and convection matrix, respectively; $[R_B^{et}]_e$, $[R_c^{et}]_e$ and $[R_s^{et}]_e$ are nodal heat flux vectors generated by external heating, convection, and conduction, respectively. They are expressed as

$$\begin{cases} [K_T^{et}]_e = \int_{S_e}([B^{et}])^T[K_\kappa][B^{et}]h\mathrm{d}S \\ [K_c^{et}]_e = \int_{\Gamma_{Sc}}([N^{et}]_e)^T\bar{\beta}[N^{et}]_e\mathrm{d}l \\ [R_B^{et}]_e = \int_{S_e}([N^{et}]_e)^T J_e h\mathrm{d}S \\ [R_c^{et}]_e = \int_{\Gamma_{Sc}}([N^{et}]_e)^T\bar{\beta}T_e\mathrm{d}l \\ [R_s^{et}]_e = \int_{\Gamma_{S_2}}([N^{et}]_e)^T q_{S_2}\mathrm{d}l \end{cases} \tag{18}$$

in which

$$[B^{et}] = \begin{bmatrix} \frac{\partial N_1^{et}}{\partial x} & \frac{\partial N_2^{et}}{\partial x} & \cdots & \frac{\partial N_M^{et}}{\partial x} \\ \frac{\partial N_1^{et}}{\partial y} & \frac{\partial N_2^{et}}{\partial y} & \cdots & \frac{\partial N_M^{et}}{\partial y} \end{bmatrix}, \quad [K_\kappa] = \begin{bmatrix} \kappa_{\mathrm{Ph}} & 0 \\ 0 & \kappa_{\mathrm{Ph}} \end{bmatrix} \tag{19}$$

The global finite element equations are obtained by assembling the elemental stiffness matrix $[C^{et}]_e$, $[K^{et}]_e$ and the right-hand-side array $[R^{et}]_e$ as

$$[C^{et}][\frac{\partial T}{\partial t}]+[K^{et}][T]=[R^{et}] \tag{20}$$

3. Results and Discussion

Suppose that a GaN-based nanofilm is subjected to a compressive prestress of 10 GPa, as shown in Fig. 1. For a nanofilm under a pulsed heat source, only the convective boundary conditions are considered and the evolution of the temperature field is solved by the Crank-Nicolson method. The initial/room temperature is 293 K in our setting. Other geometric and physical parameters of the film are given in Table 1 [51-53].

3.1. Heat Transfer in Nanofilm under Multiple Heat Pulses

In this subsection, we analyze the heat transfer behavior of stressed-nanofilm under the multiple heat pulses. The results are shown in Fig. 2(a). Three different amplitudes of heat pulse are selected to compare the influence of stress-dependent thermal conductivity on temperature response at the center of the plate, as shown in Fig. 2(b). It is found that the multiple heat pulses make the film temperature fluctuate with an increasing trend. The peak value of temperature increases with the number of heat pulse, and the attenuation of temperature in the film is slow. In this case, the temperature difference caused by the stress effect on thermal conductivity can be 8.2 K, which is about 1.8% of the peak temperature.

To have a clearer demonstration of the stress coupling effect, we show the distribution of temperature difference in Fig. 3(a) with the heat pulse amplitude of 1.5×10^{11} W/m^3. The temperature distributions at the peak times of 0.1788 s and 0.1789 s under two circumstances (*i.e.*, with and without stress coupling effect) are compared. As shown in Fig. 3(a), the increase in the number of pulse makes the overall temperature of the film higher, and the heat quickly spreads to the edge of the film. At the same time, the increase in the pulse number enhances the stress effect on thermal conductivity, which leads to a more significant temperature difference of 8.2 K. The temperature difference expands from the central region to the edges of the film. Figure 3(b) shows the distribution of thermal stress at a peak time for the case of stress-dependent thermal conductivity. Thermal stress is zero in the region where the in-plane temperature has not risen. Compared with the case of single-pulse heat source, Fig. 3(b) shows that heat diffuses further significantly as the pulse number increases, and thermal stress is generated in more regions. The maximum magnitude of thermal stress increases sharply and can be around 300 MPa.

3.2. Heat Transfer in a Nanofilm under Different Prestresses

In previous subsections, the stress coupling effect on the thermal conductivity of a GaN-based nanofilm has been discussed with the fixed in-plane prestress of -10 GPa. To explore the influence of different prestresses, we consider the prestresses of -5 GPa and -1 GPa with the same initial and boundary conditions. Figure 4 shows the temperature variation of the loaded region resulted from a multi-pulsed heat source with an amplitude of 1.5×10^{11} W/m^3 under different prestresses. If the effect of stress on thermal conductivity is neglected, the prestress does not affect temperature response speed and peak magnitude. When the stress coupling effect is considered, the negative prestress increases the thermal conductivity of the film, reduces the peak magnitude of the temperature response, and accelerates heat spreading, as shown in

Fig. 4. It is clear that as the compressive stress decreases, the influence of stress-dependent thermal conductivity on the temperature response turns weaker. The difference (with and without stress coupling effect) becomes negligible when the prestress is -1 GPa.

Figure 5 shows the distributions of temperature difference with and without stress effect on thermal conductivity under different prestresses. It is noted that the temperature difference induced by the stress coupling effect can be 8.2 K for the prestress of -10 GPa and only 1 K for the prestress of -1 GPa. It is not difficult to find that when the compressive stress is greater than 5 GPa, the thermal conductivity is significantly affected by the stress, and the coupling effect has a nontrivial contribution to heat spreading. When the compressive stress is smaller than 1 GPa, the effect of stress on thermal conductivity turns weaker, and the influence of stress-dependent thermal conductivity on the heat transfer behavior is negligible.

4. Conclusion

In this work, the influence of stress-dependent thermal conductivity on the heat transfer behavior of GaN-based nanofilm under a pulsed heat source is studied numerically. The finite element method is used to solve the temperature and stress distributions of a prestressed nanofilm. The stress coupling effect on the heat transfer behavior of the film is analyzed. The numerical results have shown that the peak temperature of the film considering the stress coupling effect is significantly higher than that of the case ignoring the stress coupling effect, and the maximum temperature difference can reach 8.2 K. The increase in pulse number not only increases the peak magnitude of temperature at the loaded point but also increases the stabilized temperature value after attenuation. The increase of pulse number also increases the in-plane thermal stress, and thus further influences the thermal conductivity of the film. Moreover, the stress coupling effect on the heat transfer behavior becomes negligible when the prestress is less than 1 GPa. These results could provide theoretical support for the optimal design of reliable GaN-based electronic devices. It should be emphasized that the numerical simulation for a heat transfer behavior is easy in comparison with experimental measurements of temperature variation in a stressed thin film. However, the latter must be conducted to validate the numerical model proposed in this work, which should be performed in future work.

Acknowledgement

This research is supported by the National Natural Science Foundation of China (Grant nos. 11772294, 11621062), and the Fundamental Research Funds for the Central Universities (Grant no. 2017QNA4031).

Reference

[1] Yanagihara, M., Uemoto, Y., Ueda, T., Tanaka, T., and Ueda, D., 2009, “Recent advances in GaN transistors for future emerging applications,” Phys. Status Solidi A, 206(6), pp. 1221-1227.

[2] Polyakov, A. Y., Smirnov, N. B., Govorkov, A. V., Markov, A. V., Kozhukhova, E. A., Gazizov, I. M., Kolin, N. G., Merkurisov, D. I., Boiko, V. M., Korulin, A. V., Zalyetin, V. M., Pearton, S. J., Lee, I. H., Dabiran, A. M., and Chow, P. P., 2009, “Alpha particle detection with GaN Schottky diodes,” J. Appl. Phys., 106(10), pp.

2273-2233.

[3] Pearton, S. J., Ren, F., Wang, Y. L., Chu, B. H., Chen, K. H., Chang, C. Y., Lim, W., Lin, J. S., and Norton, D. P., 2010, “Recent advances in wide bandgap semiconductor biological and gas sensors,” Prog. Mater Sci., 55(1) pp. 1-59.

[4] Bulgrin, K.E., Ju, Y.S., Carman, G.P., and Lavine, A.S., 2011,“An Investigation of a Tunable Magnetomechanical Thermal Switch,” ASME J. Heat Transfer, 133, p. 101401.

[5] Lu, M., Zhang, G.G., Fu, K.,Yu, G. H., Su, D., and Hu, J. F., 2011, “Gallium Nitride Schottky betavoltaic nuclear batteries,” Energy Convers. Manage., 52(4), pp. 1955-1958.

[6] Pengelly, R. S., Wood, S. M., Milligan, J. W., Sheppard, S.T., and Pribble, W. L., 2012 “A review of GaN on SiC high electron-mobility power transistors and MMICs,” IEEE Trans. Microw. Theory Tech., 60(6), pp. 1764-1783.

[7] Wang, J. H., Mulligan, P., Brillson, L., and Cao, L. R., 2015, “Review of using gallium nitride for ionizing radiation detection,” Appl. Phys. Rev., 2(3), pp. 031102.

[8] Lee, F. C. Y., Li, Q., Fei, C., and Yang, Y. C., 2019, “Applications of GaN power devices” in book Wide Bandgap Semiconductor Power Devices. Elsevier, 8, pp. 301-343.

[9] Sharma, P., and Wheeler L. T., 2007, “Size-dependent elastic state of ellipsoidal nano-inclusions incorporating surface/interface tension,” J. Appl. Mech., 74, pp. 447-454.

[10] Sun, C. Q., 2009, "Thermo-mechanical behavior of low-dimensional systems: The local bond average approach," Prog. Mater Sci., 54(2), pp.179-307.

[11] Zhu, L. L., and Zheng, X. J., 2010, "Modification of the elastic properties of nanostructures with surface charges in applied electric fields," Eur. J. Mech. A-Solids, 29, pp. 337-347.

[12] Wang, J. X., Huang, Z. P., Duan, H. L., Yu, S.W., Feng, X. Q., Wang, G.F., Zhang, W.X., and Wang, T.J., 2011, "Surface stress effect in mechanics of nanostructured materials," Acta Mech. Solida Sinica, 24, pp. 52-82.

[13] Javili, A., Mcbride, A., and Steinmann, P., 2013, "Thermomechanics of Solids With Lower-Dimensional Energetics: On the Importance of Surface, Interface, and Curve Structures at the Nanoscale. A Unifying Review," Appl. Mech. Rev., 65(1), p.010802.

[14] Zhu L. L., and Ruan, H. H., 2014, "Influence of prestress fields on the phonon thermal conductivity of GaN nanostructures," ASME J. Heat Transfer, 136, p.102402 .

[15] Huang, Z. W., Wang, Y., Zhu, J., Yu, J. R., and Hu Z.M., 2018, "Surface engineering of nanosilica for vitrimer composites," Compos. Sci. Tech., 154, pp.18-27.

[16] Morteza, K. , and Shahidi, A. R., 2019, "A general comparison the surface layer degree on the out-of-phase and in-phase vibration behavior of a skew double-layer magneto-electro-thermo-elastic nanoplate," Appl. Phys. A, 125, p. 106.

[17] Avenas, Y., Dupont, L., and Khatir, Z., 2012, "Temperature measurement of power semiconductor devices by thermo-sensitive electrical parameters-a review," IEEE Trans. Power Electron., 27(6), pp. 3081-3092.

[18] Norris, P.M., Le, N.Q., and Baker, C.H., 2013, "Tuning Phonon Transport: From Interfaces to Nanostructures," ASME J. Heat Transfer, 135, p. 061604.

[19] Chou, P. C., Cheng, S., and Chen, S. H., 2014, "Evaluation of thermal performance of all-gan power module in parallel operation," Appl. Therm. Eng., 70(1), pp. 593-599.

[20] Jones, J. P., Heller, E., Dorsey, D., and Graham, S., 2015, "Transient stress characterization of AlGaN/GaN HEMTS due to electrical and thermal effects," Microelectron. Reliab., 55 (12), pp. 2634-2639.

[21] Joglekar, S., Lian, C., Baskaran, R., Zhang, Y., Palacios, T., and Hanson, A., 2016, "Finite element analysis of fabrication- and operation-induced mechanical stress in AlGaN/GaN transistors," IEEE Trans. Semicond. Manuf., 29(4), pp. 349-354.

[22] Li, S.C., Chen, W.C., Luo, Y.D., Hu, J., Guo, P.Q., Ye, J.C., Kang, K., Chen, H.S., Li, E.P., and Yin, W. Y., 2017, "Fully coupled multiphysics simulation of crosstalk effect in bipolar resistive random access memory," IEEE Trans. Electron Devices, 64(9), pp. 3647-3653.

[23] Oh, S. K., Lundh, J. S., Shervin, S., Chatterjee, B., Lee, D. K., Choi, S., Kwak, J. S., and Ryou, J. H., 2019, "Thermal Management and Characterization of High-Power Wide-Bandgap Semiconductor Electronic and Photonic Devices in Automotive Applications," J. Electron. Packing, 141, p. 020801.

[24] Souto, J., Pura, J. L., and Jimenez, J., 2019, "Thermomechanical issues of high power laser diode catastrophic optical damage," J. Phys. D: Appl. Phys., 52, p. 343002.

[25] Calame, J. P., Myers, R. E., Wood, F. N., and Binari, S. C., 2005, "Simulations of direct-die-attached microchannel coolers for the thermal management of GaN-on-SiC microwave amplifiers," IEEE Trans. Compon. Packag. Technol., 28(4), pp. 797-809.

[26] Bykhovski, A., Gelmont, B., and Shur, M., 1993, "The influence of the strain- induced electric field on the charge distribution in GaN- AlN- GaN structure," J. Appl. Phys., 74(11), pp. 6734-6739.

[27] Rivera, C., 2011, "Effects of electrostatic force on piezoelectric materials under high electric field: Impact on GaN-based nanoscale structures," J. Appl. Phys., 109(1), p. 013513.

[28] Wang, X. P., Yin, W. Y., and He, S., 2010, "Multiphysics characterization of transient electrothermomechanical responses of through-silicon vias applied with a periodic voltage pulse," IEEE Trans. Electron Devices, 57(6), pp. 1382-1389.

[29] Ancona, M. G., Binari, S. C., and Meyer, D. J., 2012, "Fully coupled thermoelectromechanical analysis of GaN high electron mobility transistor degradation," J. Appl. Phys., 111(7), p. 074504.

[30] Zhang, R., Zhao, W., and Yin, W. Y., 2014, "Investigation on thermo-mechanical responses in high power multi-finger AlGaN/GaN HEMTs," Microelectron. Reliab., 54(3), pp. 575-581.

[31] Zhang, R., Zhao, W. S., Yin, W. Y., Zhao, Z. G., and Zhou, H. J., 2015, "Impacts of diamond heat spreader on the thermo-mechanical characteristics of high-power AlGaN/GaN HEMTs," Diamond and Relat. Mater., 52, pp. 25-31.

[32] Abramson, A. R., Tien, C. L., and Majumdar, A., 2002, "Interface and Strain Effects on the Thermal Conductivity of Heterostructures: A Molecular Dynamics Study," ASME J. Heat Transfer, 124(5), pp. 963–970.

[33] Picu, R. C., Borca-Tasciuc, T., and Pavel, M. C., 2003, "Strain and Size Effects on Heat Transport in Nanostructures," J. Appl. Phys., 93, pp. 3535–3539.

[34] Zhu, L. L., and Zheng, X. J., 2009, "Modification of the phonon thermal conductivity in spatially confined semiconductor nanofilms under stress fields," Europhys. Lett., 88, p. 36003.

[35] Li, X. B., Maute, K., Dunn, M. L., and Yang, R. G., 2010, "Strain Effects on the Thermal Conductivity of Nanostructures," Phys. Rev. B, 81, p. 245318.

[36] Jung, K., Cho, M., and Zhou, M., 2011, "Strain Dependence of Thermal Conductivity of [0001]-Oriented GaN Nanowires," Appl. Phys. Lett., 98, p. 041909.

[37] Alam, M. T., Manoharan, M. P., Haque, M. A., Muratore, C., and Voevodin, A., 2012, "Influence of Strain on Thermal Conductivity of Silicon Nitride Thin Films," J. Micromech. Microeng., 22, p. 045001.

[38] Luo, H. N. and Zhu, L. L., 2015, "Effects of surface stress on the phonon properties in GaN nanofilms," ASME J. Appl. Mech., 82, p. 111002.

[39] Zhu, L. L., and Luo, H. N., 2016, "Phonon properties and thermal conductivity of

GaN nanofilm under prestress and surface/interface stress," J. Alloys Compd., 685, pp.619-625.

[40] Wang, J. C., Zhu, L. L., and Yin, W. Y., 2018, "Effects of heterogeneity and prestress field on phonon properties of semiconductor nanofilms," Comp. Mater. Sci., 145, pp. 14-23.

[41] Zhu, L. L., Tang, X. Y., Wang, J. C., and Hou, Y., 2019, "Modeling phonon thermal conductivity in spatially confined GaN nanofilms under stress fields and phonon surface scattering," AIP Adv., 9, p. 015024.

[42] Tang, X. Y., Wang, J. C., Zhu, L. L., and Yin, W. Y., 2019, "Simulating stress-tunable phonon and thermal properties in heterostructgured AlN/GaN/AlN-nanofilms," Mater. Res. Express, 6, p. 015018.

[43] Zhang, S. Y., Tang, X. Y., Ruan, H. H., and Zhu, L. L., 2019, "Effects of surface/interface stress on phonon properties and thermal conductivity in AlN/GaN/AlN heterostructural nanofilms," Appl. Phys. A, 125, p.732.

[44] Bannov, N., Aristov, V., and Mitin, V., 1995, "Electron Relaxation Times Due to the Deformation-Potential Interaction of Electrons With Confined Acoustic Phonons in a Free-Standing Quantum Well," Phys. Rev. B, 51, pp. 9930–9942.

[45] Balandin, A., and Wang, K. L., 1998, "Significant Decrease of the Lattice Thermal Conductivity Due to Phonon Confinement in a Free-Standing Semiconductor Quantum Well," Phys. Rev. B, 58, pp. 1544–1549.

[46] Zou, J., Lange, X., and Richardson, C., 2006, "Lattice Thermal Conductivity of Nanoscale AlN/GaN/AlN Heterostructures: Effects of Partial Phonon Spatial

Confinement," J. Appl. Phys., 100, p. 104309.

[47] Zhu, L. L., and Zheng, X. J., 2009, "Modification of the phonon thermal conductivity in spatially confined semiconductor nanofilms under stress fields," Europhys. Lett., 88, p. 36003.

[48] Balandin, A. A., Pokatilov, E. P., and Nika, D. L., 2007, "Phonon Engineering in Hetero- and Nanostructures," J. Nanoelectron. Optoelectron., 2, pp. 140–170.

[49] Wedler, G., Walz, J., Hesjedal, T., Chilla, E. and Koch, R., 1998, "Stress and Relief of Misfit Strain of Ge/Si(001)," Phys. Rev. Lett., 80, p. 2382.

[50] Chang, C. L., Jaob, J. Y., Hoa, W. Y. and Wang, D. Y., 2007, "Influence of bi-layer period thickness on the residual stress, mechanical and tribological properties of nanolayered TiAlN/CrN multi-layer coatings,"Vacuum, 81, pp.604-609.

[51] Sichel, E. K., and Pankove, J. I., 1977, "Thermal Conductivity of GaN, 25–360 K," J. Phys. Chem. Solids, 38, p. 330.

[52] Zou, J., 2010, "Lattice Thermal Conductivity of Freestanding Gallium Nitride Nanowires," J. Appl. Phys., 108, p. 034324.

[53] AlShaikhi, A., Barman, S., and Srivastava, G. P., 2010, "Theory of the Lattice Thermal Conductivity in Bulk and Films of GaN," Phys. Rev. B, 81, p. 195320.

Table 1. Geometric and physical parameters of GaN-based films

Length	Width	Thickness	Convection coefficient	Specific heat • density
a (m)	b (m)	h (m)	$\bar{\beta}$ (W/m^{2}K)	$c\rho$ (J/m^{3}K)
0.005	0.005	6×10^{-9}	50	AlN 1.02×10^{5} GaN 2.23×10^{5}

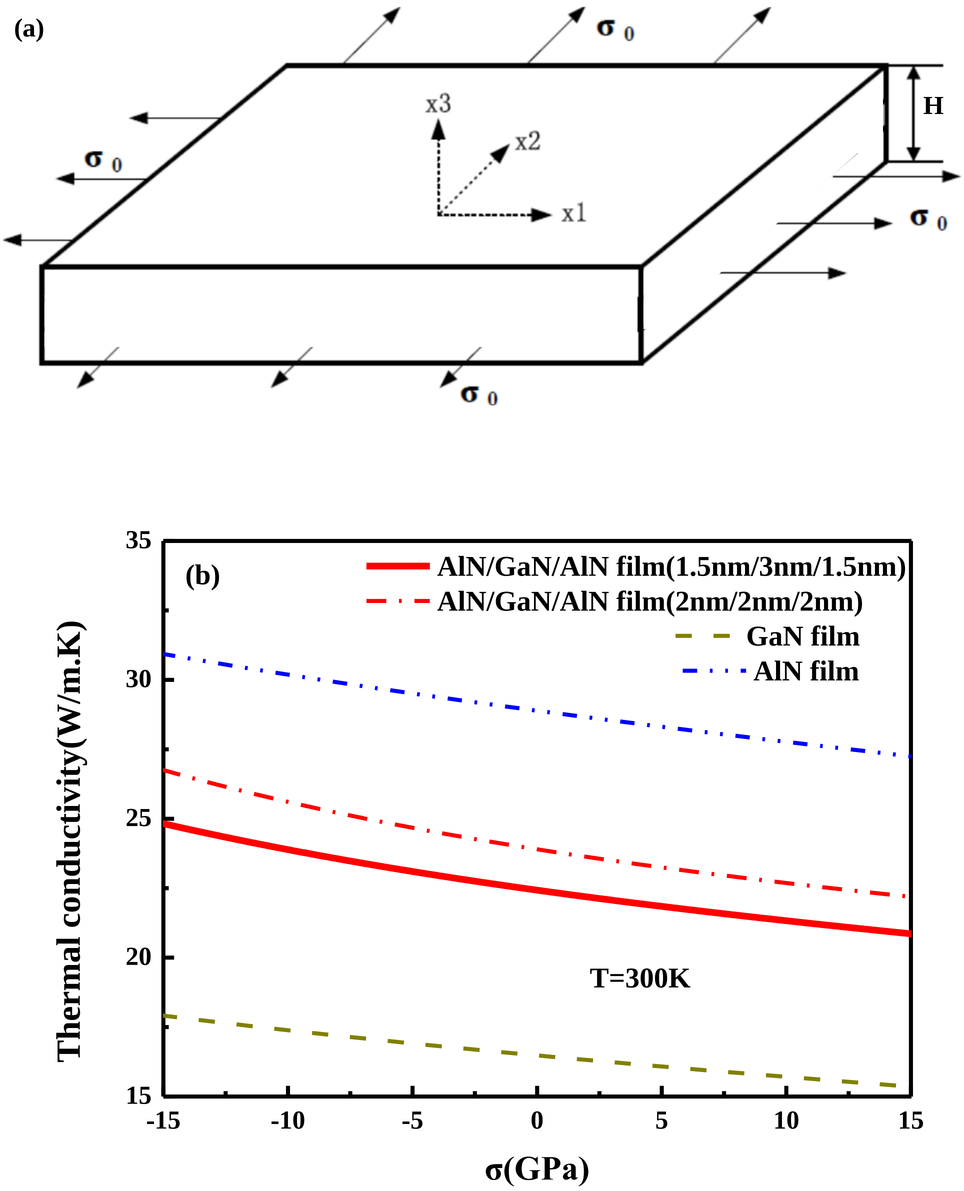

Fig. 1. Schematic diagram of prestressed nanofilm (a), and the simulated phonon thermal conductivity varying with the prestress for GaN-based nanofilm (b).

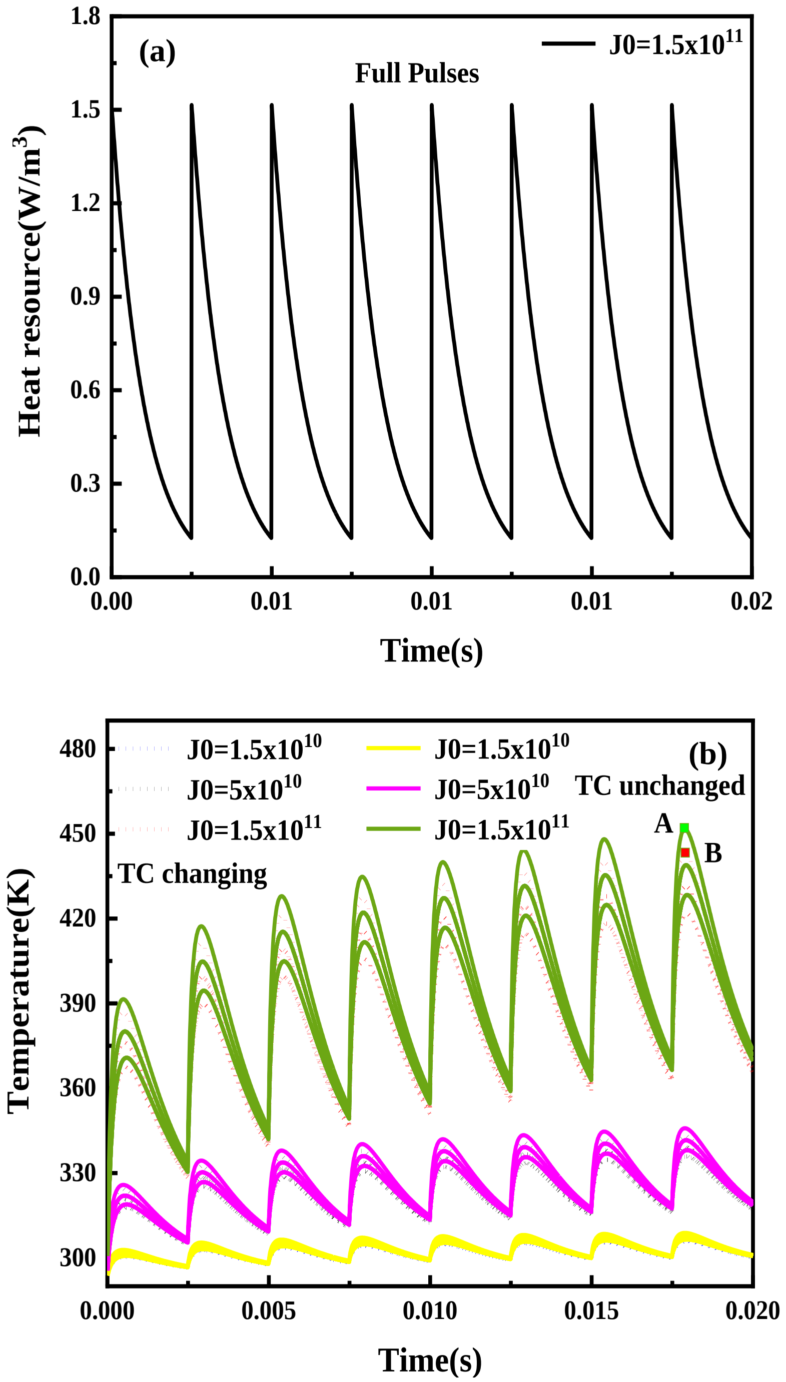

Fig. 2. The heat flow varying with time for the multiple pulse heat source (a), and the temperature responses of nanofilm at all loading points under different pulse intensities with (dotted line) and without (solid line) stress coupling effect of thermal conductivity (b) (The letters A and B in the figure, respectively, mark the corresponding peak temperature moments of t=0.1788 s and t=0.1789 s).

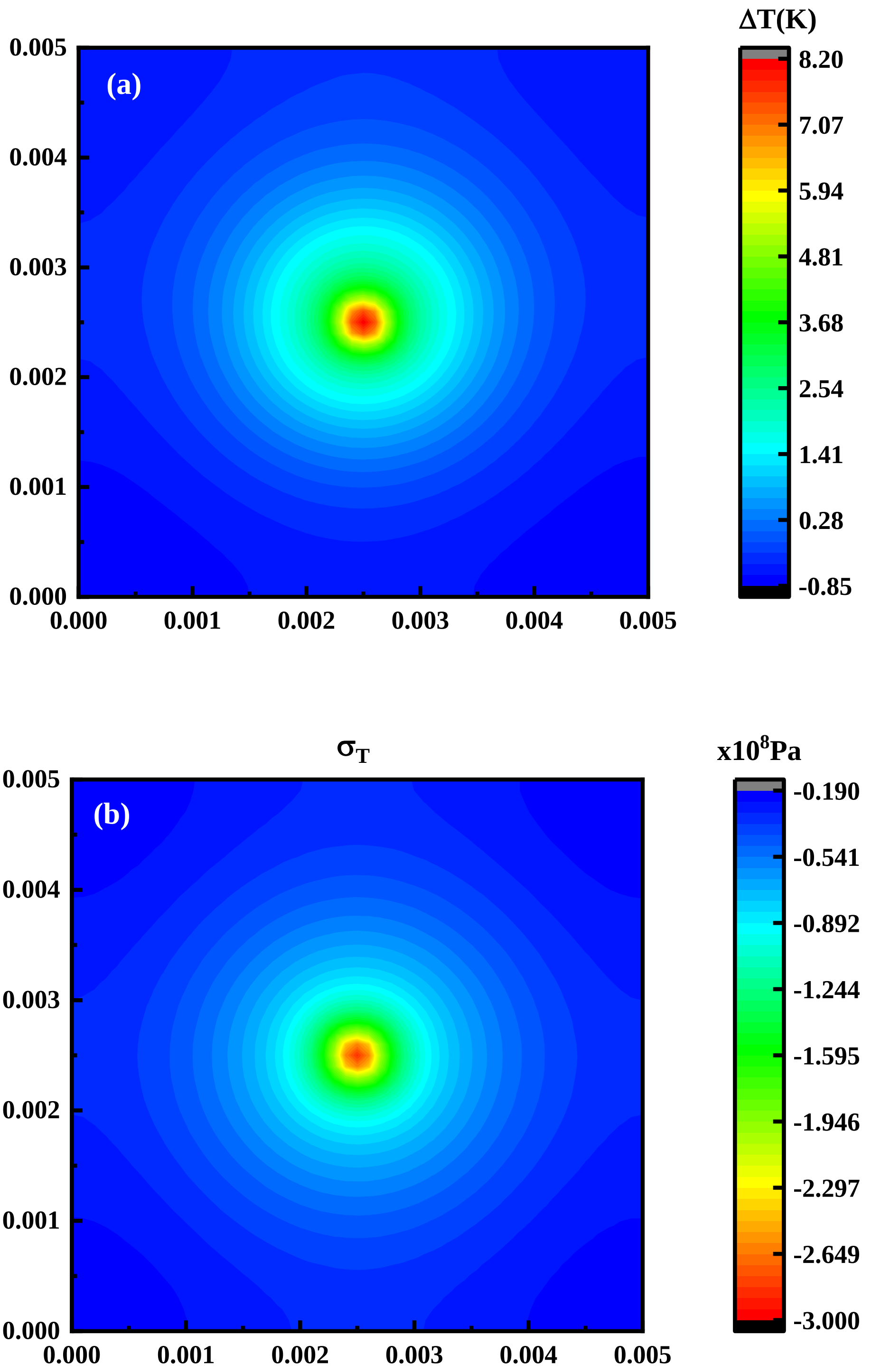

Fig. 3. Temperature distributions under multiple heat pulses with stress-dependent thermal conductivity (a), and distributions of thermal stress under multi-pulsed heat source considering stress coupling effect at t=0.1788 s (b).

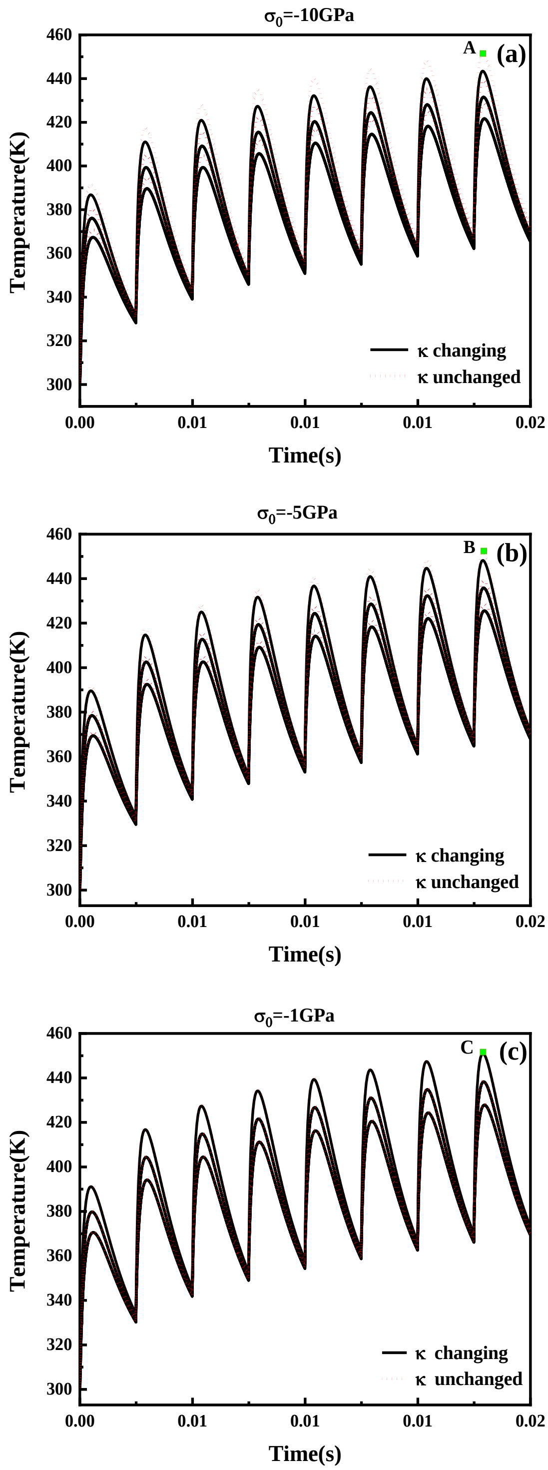

Fig. 4. Temperature response curves of heat loading points with two cases of considering and neglecting the stress coupling effect under different prestresses (the letters A, B and C in the figure, respectively, mark the corresponding peak temperature moments for $t_A = 0.1788$ s, $t_B = 0.1789$ s and $t_C = 0.1789$ s).

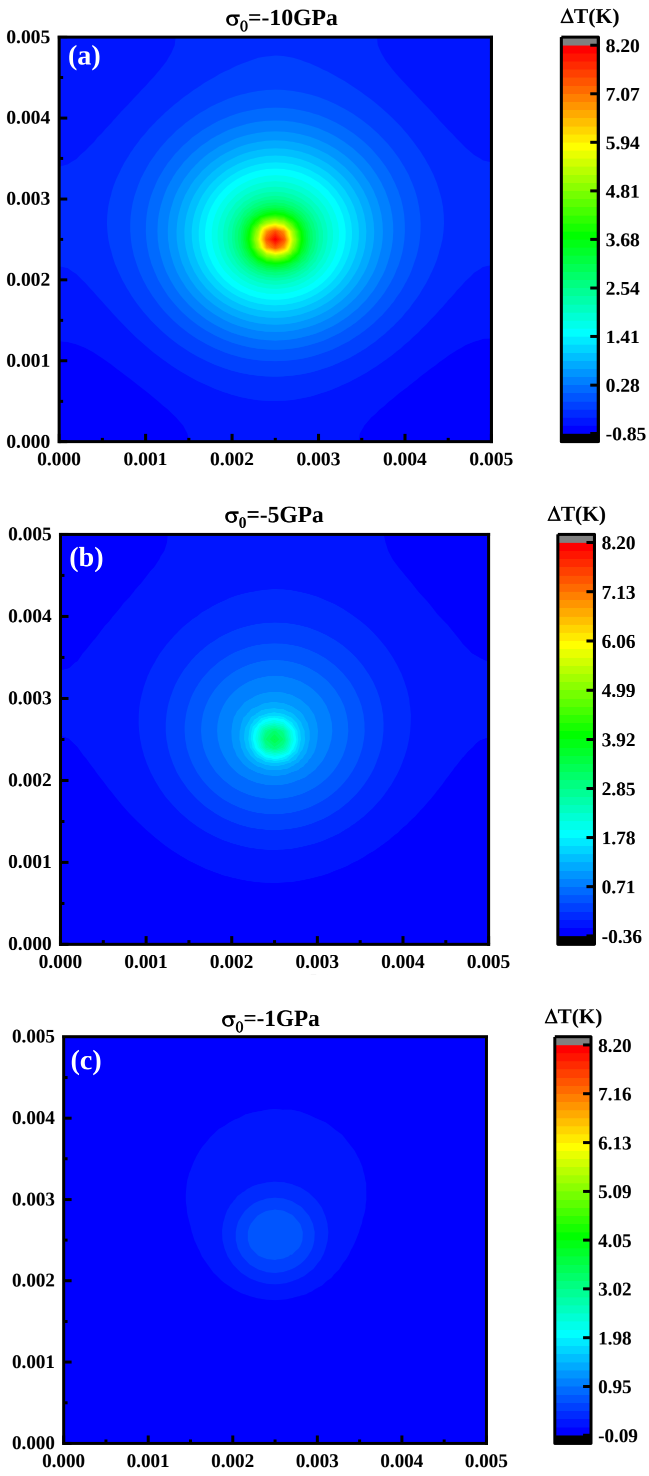

Fig. 5. The distributions of temperature difference under different prestresses through comparing the cases of considering and neglecting the stress coupling effect of thermal conductivity.